

PoseMaster: A Unified 3D Native Framework for Stylized Pose Generation

Hongyu Yan^{1,2*} Kunming Luo^{1*} Weiyu Li¹ Kaiyi Zhang^{1,2}
 Yixun Liang¹ Jingwei Huang² Chunchao Guo^{2†} Ping Tan^{1†}

¹Hong Kong University of Science and Technology ²Tencent Hunyuan
 {hyanar, kluoad}@connect.ust.hk, pingtan@ust.hk



Figure 1. Given a single image and arbitrary poses represented by a 3D skeleton, PoseMaster can generate a high-quality 3D asset that maintains the identity of the image while adhering to the pose defined by the skeleton, enabling rich and precise 3D pose stylization.

Abstract

Pose stylization, which aims to synthesize stylized content aligning with target poses, serves as a fundamental task across 2D, 3D, and video domains. In the 3D realm, prevailing approaches typically rely on a cascade pipeline: first manipulating the image pose via 2D foundation models and subsequently lifting it into 3D representations. However, this paradigm limits the precision and diversity of the 3D pose stylization. To this end, we propose a novel paradigm for 3D pose stylization that unifies pose stylization and 3D generation within a cohesive framework. This integration minimizes the risk of cumulative errors and enhances the model’s efficiency and effectiveness. In addition, diverging from previous works that typically utilize 2D skeleton images as guidance, we directly utilize the 3D skeleton because it can provide a more accurate representation of 3D spatial and topological relationships, which significantly enhances the model’s capacity to achieve richer

and more precise pose stylization. Moreover, we develop a scalable data engine to construct a large-scale dataset of “Image-Skeleton-Mesh” triplets, enabling the model to jointly learn identity preservation and geometric alignment. Extensive experiments demonstrate that PoseMaster significantly outperforms state-of-the-art methods in both qualitative and quantitative metrics. Owing to the strict spatial alignment between the generated 3D meshes and the conditioning skeletons, PoseMaster enables the direct creation of animatable assets when coupled with automated skinning models, highlighting its compelling potential for automated character rigging.

1. Introduction

With the burgeoning demand for digital content in gaming, film production, and virtual reality, the ability to generate stylized assets that maintain unified Intellectual Property (IP) consistency has become paramount. While significant strides have been made in 2D and video generation, 3D pose stylization—the task of generating 3D assets that

*Equal contribution.

†Corresponding authors.

strictly align with a target pose while preserving specific visual styles—remains a formidable challenge. Although recent 3D native generative models have demonstrated the capacity to synthesize high-quality geometry from a single image, controlling these generations with precise pose guidance continues to be an underexplored frontier.

Prevailing approaches typically treat 3D pose stylization as a decoupled process, combining 2D pose manipulation with subsequent 3D lifting. Methods such as CharacterGen [47], StdGen [19], and SKDream [61] rely heavily on a cascade pipeline: they first employ 2D controllable models (e.g., ControlNet [70]) to generate a stylized image guided by a 2D skeleton image, and then utilize a separate reconstruction model to lift this image into a 3D asset. Despite their popularity, these cascade paradigms suffer from two fundamental limitations. First, error propagation is inevitable; artifacts, occlusions, or inconsistencies introduced during the 2D generation phase are directly amplified in the 3D reconstruction, leading to geometric distortions. Second, relying on 2D skeleton images introduces inherent geometric ambiguity. A 2D projection loses critical depth information and spatial relationships, making it difficult to resolve self-occlusions or complex topological structures, thereby limiting the precision of the final 3D pose.

To bridge this gap, we present PoseMaster, a novel 3D native framework that unifies pose stylization and 3D generation within a single, end-to-end generative model. Diverging from the conventional reliance on 2D skeleton images, we propose to explicitly leverage 3D skeletons as the control signal. Unlike 2D representations which suffer from projection ambiguity, 3D skeletons provide explicit spatial coordinates and topological relationships, offering a robust geometric prior for the generation process. To harness this, we design a specialized 3D skeleton encoder capable of capturing fine-grained structural details. This design enables PoseMaster to bypass the limitations of the 2D-lifting paradigm, minimizing cumulative errors and ensuring that the generated 3D assets are precisely aligned with the target pose while maintaining high-fidelity identity preservation.

However, training such a 3D native model presents a significant data challenge: there is a scarcity of large-scale, high-quality paired data containing “Image-Skeleton-3D Mesh” triplets. Naive solutions, such as utilizing existing animatable datasets like ReadyPlayerMe [3] or VRoid [7], often fall short in terms of stylistic diversity and quantity. To address this bottleneck, we introduce a scalable Data Engine designed to construct a massive dataset of stylized 3D assets by introducing both static and animated 3D assets, which enables the model to jointly learn the correlation between visual appearance (ID) and geometric structure (Pose), significantly enhancing its generalization capabilities across diverse styles and complex poses.

Extensive evaluations demonstrate that PoseMaster es-

tablishes a new state-of-the-art in both pose canonicalization and arbitrary-pose stylization. Crucially, the 3D meshes generated by our framework exhibit precise spatial alignment with the conditioning 3D skeletons. This inherent spatial consistency naturally yields rigged assets that can be seamlessly skinned and animated, entirely bypassing the need for time-consuming manual skeleton retargeting and post-processing.

- We propose PoseMaster, a novel 3D native generation paradigm for pose stylization, which integrates pose stylization and 3D geometry generation into a cohesive framework, effectively eliminating the error propagation inherent in traditional cascade pipelines.
- We introduce a novel 3D-skeleton-based control mechanism and a scalable data engine. By capturing explicit spatial and topological relationships from 3D skeletons and training on large-scale “Image-Skeleton-Mesh” triplets, we significantly enhance the model’s precision and generalization ability.
- We demonstrate that our method achieves state-of-the-art performance in both qualitative and quantitative evaluations. Furthermore, we validate the practical value of our framework by showing that it generates rigged assets to facilitate the animatable character creation.

2. Related work

2.1. 2D Pose Stylization

Pose stylization is a longstanding research challenge in the field of image and video generation. Recent advances, such as image diffusion models like Stable Diffusion [50], have inspired methods that incorporate a 2D skeleton condition to achieve pose stylization. Notable examples include ControlNet [70] and its variants [46, 59, 74, 75], which utilize skeletons derived from Openpose [10] for pose control. However, these methods are limited to constraining the content generated by text-to-image (T2I) models and do not allow for editing poses in existing images. While Vision-Language Models such as Qwen-Image [55], GPT-4o [1], NanoBanala [2], and Seed [6] can synthesize and edit poses from text or image prompts, achieving rich pose stylization while preserving identity remains challenging. In the domain of video generation, several methods [21, 53, 54, 60] employ skeleton sequences to create animation videos. Inspired by these, this paper aims to advance 3D pose stylization in the 3D generation framework.

2.2. 3D Pose Stylization

Early 3D pose stylization approaches [9, 23, 25, 37, 68, 70, 73] often rely on 2D stable diffusion priors and human geometry priors from models like SMPL or Openpose [10] to constrain generated 3D humans. While these text-based generation models exhibit impressive controllability, they

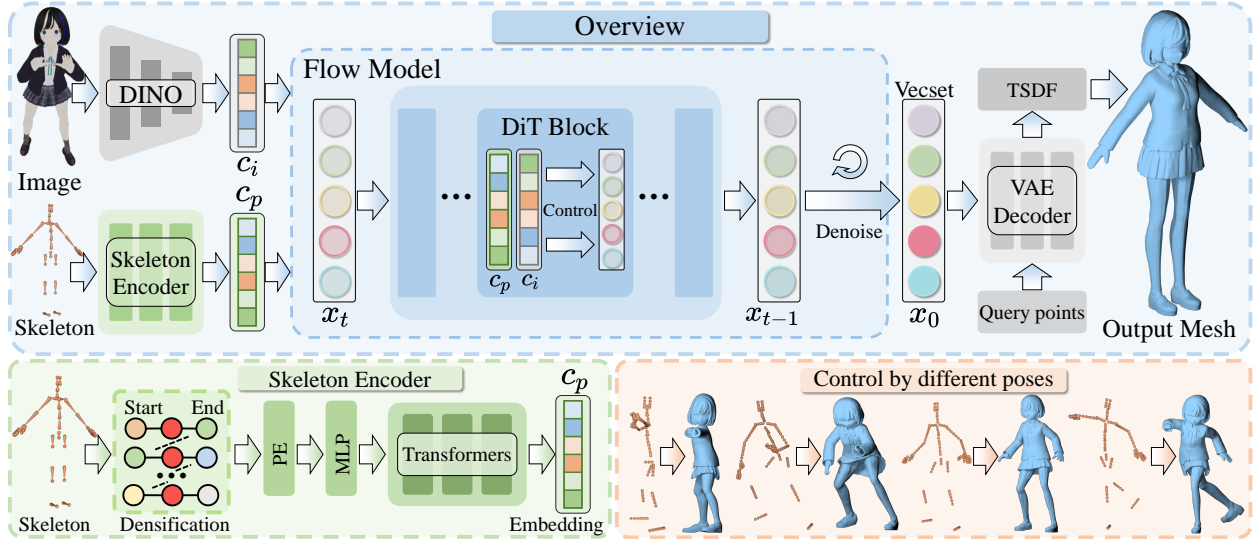


Figure 2. Overall pipeline of our PoseMaster. Given a single image and a 3D skeleton, our PoseMaster integrates them into a unified 3D native generation framework to achieve precise pose stylization under 3D generation.

strictly rely on textual descriptions for character specification, thereby lacking support for more intuitive visual or spatial input modalities. To address this, CharacterGen [47] introduced an image-driven pipeline for controllable character generation by converting arbitrary-pose images into A-pose multi-view images using multi-view diffusion models [31, 41, 42], followed by reconstruction of A-pose 3D characters through a multi-view-based LRM [20]. Building on CharacterGen, StdGen [19] and SKDream [61] enhance geometric quality and controllability. However, these approaches depend on 2D models for pose stylization, which can lead to identity and texture distortion and cumulative errors. In this paper, we propose a native paradigm for cohesive pose stylization and 3D generation, achieving superior geometric quality and control accuracy.

2.3. 3D Native Generation

3D native generation methods utilize representations such as point clouds [30, 65, 78], meshes [40, 43, 51], and implicit functions [13, 45, 49] to optimize their networks. These methods benefit from direct 3D data optimization, resulting in impressive geometric quality. The introduction of the VecSet representation by 3DShapeVecSet [67] has spurred rapid advancements in 3D native generation. Building on VecSet, models such as Michelangelo [76], Clay [71], CraftsMan [32], and Hunyuan3D 2.1 [22] have developed large 3D latent diffusion models to enhance the effectiveness and generalization of 3D generation. Recent methods [8, 12, 14, 22, 28, 29, 33, 34, 56, 57, 66] demonstrate impressive geometric quality using sparse voxel representations introduced by Trellis [58]. However, these methods often rely heavily on image alignment, limiting

their ability to enrich input data. In this paper, we advance the 3D native generation pipeline by integrating 3D skeleton conditions to achieve pose stylization while preserving the identity of the input.

3. Preliminary Study

A 3D native generation model comprises two main components: the 3D Variational Autoencoder (VAE) and the 3D Diffusion Model (DiT). The 3D VAE is employed to obtain the latent representation of geometry. For instance, in a VecSet-based VAE, given a surface input, the model first utilizes an encoder to derive the latent VecSet. Subsequently, it recovers the truncated signed distance function (TSDF) through a decoder, allowing us to leverage iso-surface extraction to obtain explicit mesh output.

Flow-based DiT [38] defines the forward process, $x_t = (1-t)x_1 + tx_0$, as straight paths between the data distribution and a standard normal distribution. In this design, the velocity v can be approximated with a neural network v_θ by minimizing the conditional flow matching objective:

$$\mathbb{E}_{t,x_0,x_1} \|v_\theta(x, t) - (x_1 - x_0)\|_2^2. \quad (1)$$

Following this, we can obtain our conditional flow matching objective:

$$\mathbb{E}_{t,x_0,x_1,c_i,c_p} \|v_\theta(x, t, c_i, c_p) - (x_1 - x_0)\|_2^2. \quad (2)$$

where c_i is image condition while c_p is pose condition.

4. Method

In this section, we begin by introducing our data construction to show how we organize our data to achieve native

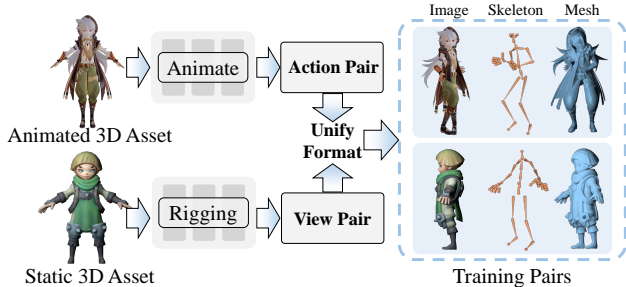


Figure 3. Overview of the dataset construction pipeline. Our approach integrates both dynamic articulated meshes and static geometries to curate a large-scale dataset consisting of strictly aligned image-skeleton-mesh triplets.

stylized pose generation in Section 4.1. Then, we present how we design our unified framework to accomplish high-quality pose stylization in Section 4.2.

4.1. Data Engine

Achieving end-to-end pose stylization within a native 3D generation framework requires a dataset of cross-pose “Image-Skeleton-Mesh” triplets, where the 3D structures (skeleton and mesh) are perfectly aligned but strictly decoupled from the reference image pose. While current methods [19, 47] construct such triplets using animatable 3D assets, this paradigm suffers from two major limitations. First, the severe scarcity of open-source animatable assets hinders the construction of datasets at scale. Second, the limited stylistic diversity of existing animatable assets restricts the model’s generalization capabilities. To overcome these bottlenecks, we introduce a scalable data engine.

Specifically, we systematically collect diverse open-source 3D datasets and rigorously filter them to extract humanoid assets. As illustrated in Figure 3, we synergize both animatable and static 3D assets to synthesize large-scale, pose-decoupled “Image-Skeleton-Mesh” triplets.

For animatable 3D assets (e.g., ReadyPlayerMe [3], VRoid [7], and Playbox [5]), we animate the characters using various motion sequences to render multi-frame images, skeletons, and meshes. To construct cross-pose pairs (denoted as Action Pairs), we sample an image from one motion frame and pair it with the spatially aligned skeleton and mesh extracted from another frame (see Figure 3).

For static 3D meshes sourced from diverse platforms like Objaverse [17], Objaverse-XL [16], and HumanRig [15], we first render multi-view images. To obtain the corresponding 3D skeletons, we adopt a dual strategy: for inherently rigged assets, we directly extract their provided skeletons, whereas for unrigged meshes, we employ an automatic rigging model to infer their skeletal structures. Subsequently, we pair a rendered image from one specific viewpoint with the fully aligned 3D skeleton and mesh to con-

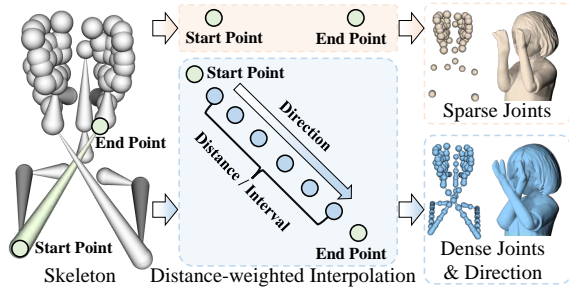


Figure 4. The skeleton representation of sparse joints and ours. We propose a distance-weighted interpolation scheme to densify the skeletal graph. Furthermore, explicit bone directional vectors are embedded into all interpolated points belonging to the same skeletal segment.

struct View Pairs, which implicitly forces the network to infer view-occluded regions.

Furthermore, we employ the watertight algorithm from Hunyuan3D 2.1 to generate watertight meshes and sample surface points. Crucially, we track the exact normalization parameters and apply identical transformations to the corresponding skeletons, thereby ensuring strict spatial registration between the geometries and their kinematic structures. Ultimately, our data engine yields a massive dataset comprising over 500K unique humanoid objects. By permuting the diverse poses and viewpoints for each object, the total volume of valid training pairs scales well into the millions.

4.2. Framework

Similar to recent 3D native generation models [32, 71], our PoseMaster consists of two primary components: a 3D Variational Autoencoder (VAE) and a 3D Diffusion Transformer (DiT), as illustrated in Figure 2. The backbone of our architecture is built upon Hunyuan3D 2.1 [22], into which we introduce a dedicated skeleton encoder to capture geometric pose constraints. Consequently, given an arbitrary reference image and a target 3D skeleton, our framework generates a high-fidelity 3D mesh that preserves the identity and appearance of the input image while strictly adhering to the pose defined by the skeleton.

4.2.1. Skeleton Encoders

The skeleton encoder plays a pivotal role in our pipeline. Previous 2D- or video-based pose stylization methods typically utilize 2D skeleton maps (e.g., Openpose [10]), which is a natural choice since their output modalities align with the 2D domain. However, for 3D native generation, relying on 2D skeletons fails to provide the network with sufficient spatial and topological awareness, inevitably leading to imprecise control. In contrast, a 3D skeleton offers an explicit geometric scaffold, significantly alleviating the complexity of geometric reconstruction in 3D generation. Thus, employing 3D skeletons as pose conditions is inherently better

suited for 3D pose stylization.

A standard 3D skeleton consists of the start and end joints of individual bones. A straightforward approach of representing the pose, as seen in previous work [72], is the 3D coordinates of sparse joints. While this adequately conveys simple poses (e.g., A-pose or T-pose), its sparsity and lack of explicit topological connectivity hinder the network’s ability to interpret complex articulations, as demonstrated in Figure 4. To address this, we propose a densification strategy to extract structural pose representations. Specifically, we perform distance-weighted interpolation along each bone—from the start joint to the end joint—to construct a dense point cloud. To ensure uniform point distribution regardless of varying bone lengths, the number of interpolated points per bone is strictly determined by its bone length and predefined spatial interval (e.g., 0.005). Furthermore, to explicitly encode topological information into this dense representation, we assign the directional vector of each bone (defined as the vector from the start to the end joint) to all sampled points belonging to that bone. Consequently, our pose representation is formulated as $P \in \mathbb{R}^{N \times 6}$, where N denotes the number of points, and each point contains both 3D coordinates and 3D directional features. Finally, we employ Farthest Point Sampling (FPS) to uniformly downsample the interpolated point cloud to a fixed size of 256 points.

To extract skeleton features, as depicted in Figure 2, we leverage a point transformer architecture to capture fine-grained spatial structures and topological relationships. Specifically, the 3D coordinates P_c are first projected into high-dimensional embeddings via a positional encoding layer, and then concatenated with the directional features P_f . A linear projection layer subsequently maps the concatenated features to a dimension of 1024, followed by two stacked point transformer blocks to derive the final skeleton condition c_p . This process is formulated as:

$$c_p = \phi_2(\phi_1(\mathcal{T}([PE(P_c), P_f]))) \quad (3)$$

where $[\cdot]$ denotes concatenation along the feature dimension, $PE(\cdot)$ represents the positional embedding, $\mathcal{T}(\cdot)$ is the linear projection layer, and ϕ_1, ϕ_2 correspond to the two point transformer blocks.

4.2.2. Multi-Condition DiT

Our PoseMaster integrates two condition encoders to process the image condition c_i and the skeleton condition c_p . For the image input I_i , following Hunyuan3D 2.1 [22], we utilize DINOv2-Large [44] at a resolution of 518 to extract the image features, formulated as $c_i = \text{DINOv2}(I_i)$. To preserve the generative priors of the foundation 3D model while allowing the skeleton condition to exert dominant control over the generated pose during training progressively, we integrate the skeleton condition c_p with the image condition c_i at the token level to form a joint condition

representation. The CFG formulation for predicting the velocity/noise v_θ is defined as follows:

$$\hat{v}_\theta = v_\theta(x_t, t, c_p, \emptyset) + \lambda \cdot (v_\theta(x_t, t, c_p, c_i) - v_\theta(x_t, t, c_p, \emptyset)) \quad (4)$$

where x_t is the noisy input at timestep t , \emptyset denotes the nullified image condition, and λ is the guidance scale.

5. Experiments

5.1. Implementation Details and Metrics

We initialize our model using the pre-trained weights of the VAE and Diffusion Transformer (DiT) from Hunyuan3D 2.1 [22]. During the fine-tuning phase, we keep the image encoder and VAE strictly frozen. We specifically focus on jointly optimizing the DiT backbone and the skeleton encoder, employing a constant learning rate of 1×10^{-5} . Furthermore, to ensure dimensional compatibility with the extracted DINO features, the skeleton conditions are projected into a 1024-dimensional feature space. To enhance the robustness and generalization of PoseMaster, we incorporate comprehensive data augmentation strategies across both 2D and 3D modalities. For the 2D image input, we apply random planar rotations $\in [-30^\circ, 30^\circ]$ with a 15% probability. For the 3D skeleton, we adopt standard point cloud augmentation techniques [48, 63, 64], encompassing random translation, scaling, and rotation. Crucially, to preserve strict spatial alignment between the driving skeleton and the target 3D mesh—a prerequisite for extracting accurate and consistent latent codes—we apply these identical 3D transformations synchronously to both the skeleton and the sampled surface points.

Regarding evaluation metrics, conventional geometric distances such as Chamfer Distance (CD) are sub-optimal for assessing 3D pose stylization. This limitation arises because generative models inherently struggle to achieve perfect spatial alignment with ground-truth (GT) meshes, particularly in high-variance (e.g., garment, hair) or occluded regions. Therefore, following recent robust surface evaluation protocols [18, 24], we evaluate surface quality using the Mean Angular Error (MAE) and Cosine Similarity (SIM) of surface normals, which effectively circumvent the errors caused by the spatial misalignment. The detailed computation pipeline is provided in the supplementary material. Furthermore, consistent with Hunyuan3D 2.1, we adopt Uni3D-I [77] and ULIP-I [62] to assess the semantic and structural alignment between the generated mesh and the GT single-view image.

5.2. Results and Comparisons

5.2.1. Comparison on Pose Canonicalization

Pose canonicalization—transforming an in-the-wild image with an arbitrary pose into a 3D mesh in a standard canon-

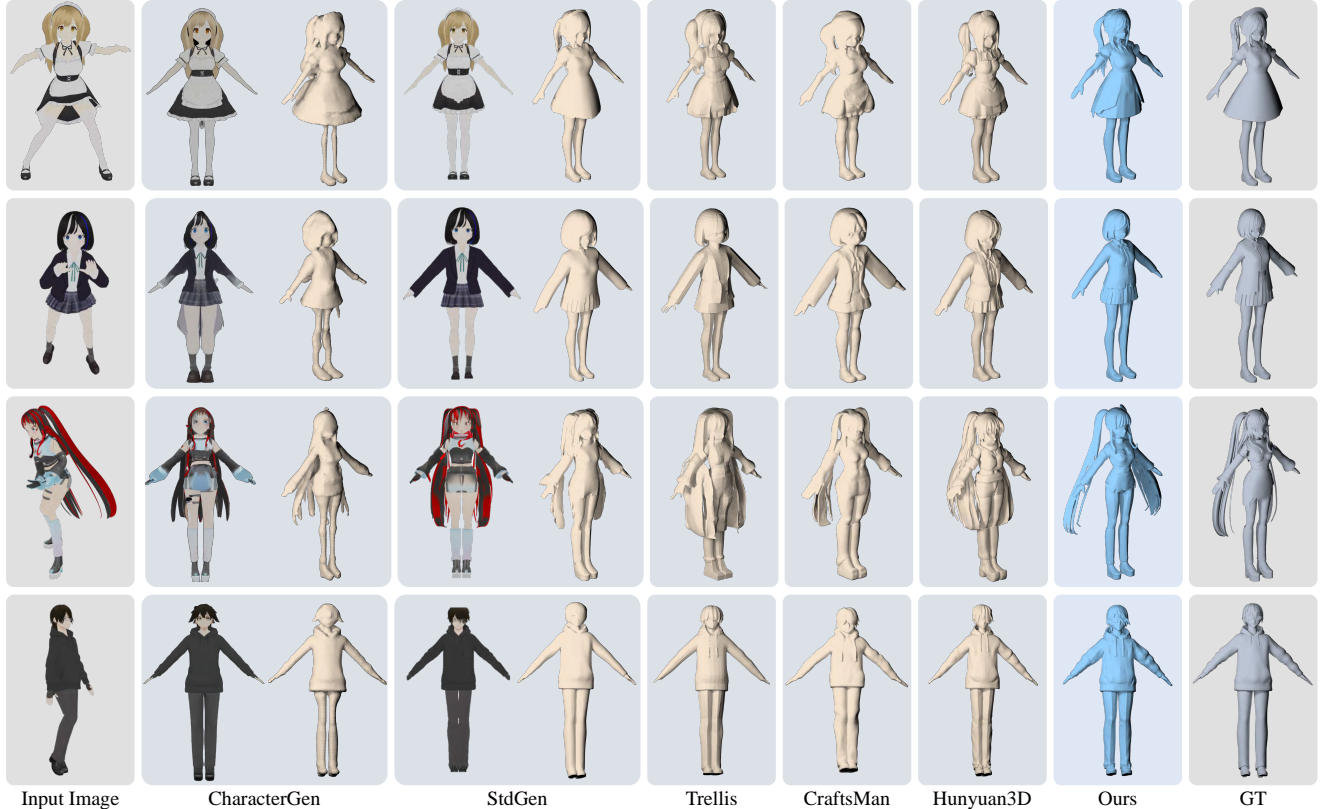


Figure 5. The qualitative comparison for pose canonicalization on VRoid [7] dataset. Our method achieves higher geometry quality and accuracy compared with baselines.

ical pose (e.g., A-pose or T-pose)—is a fundamental sub-task inherently supported by PoseMaster. We compare our approach with task-specific pipelines, CharacterGen [47] and StdGen [19]. Additionally, we include state-of-the-art 3D native generators such as CraftsMan [32], Trellis [58], and Hunyuan3D 2.1 [22]. Since these 3D native generators don’t support pose stylization, we leverage A-pose images generated from StdGen as their inputs.

To ensure a fair comparison, we evaluate 50 images with diverse poses extracted from the VRoid dataset [7], which aligns with the training distribution of CharacterGen and StdGen. As reported in Table 1, PoseMaster achieves state-of-the-art performance across all metrics. Qualitatively, Figure 5 reveals a critical flaw in cascaded pipelines: the intermediate A-pose images produced by 2D canonicalization methods (e.g., StdGen) frequently suffer from severe structural distortions and artifacts. Due to the strict image-geometry alignment priors of 3D native generators, these 2D artifacts are deterministically projected into the final 3D meshes (such as cases in the first and third rows of Figure 5), leading to significant error accumulation. In contrast, by bypassing the error-prone 2D canonicalization step and directly leveraging 3D skeleton guidance within a native gen-

Table 1. The quantitative comparison for pose canonicalization on an arbitrary-pose image from the VRoid [7] test dataset. “*” denotes that these methods leverage the image-based pose canonicalization method to obtain the A-pose image input.

Method	MAE ↓	Sim ↑	Uni3D-I ↑	ULIP-I ↑
CharacterGen [47]	6.38	0.905	0.343	0.146
StdGen [19]	4.97	0.930	0.398	0.160
Trellis [58]*	5.39	0.926	0.398	0.157
CraftsMan [32]*	5.67	0.924	0.378	0.139
Hunyuan3D 2.1 [22]*	5.89	0.920	0.398	0.150
PoseMaster (Ours)	4.59	0.938	0.402	0.161

eration workflow, PoseMaster dramatically preserves the identity of the input and yields highly reliable geometry.

5.2.2. Comparison on Arbitrary-pose Stylization

Beyond canonicalization, our method excels at arbitrary pose stylization. However, directly comparing with existing literature is challenging, as 2D image-based methods (e.g., SKDream [61], ControlNet [70]) and video-based methods [21, 54] primarily rely on 2D Openpose-style skeleton as an additional condition for achieving image pose editing, making it difficult to run a fair comparison.

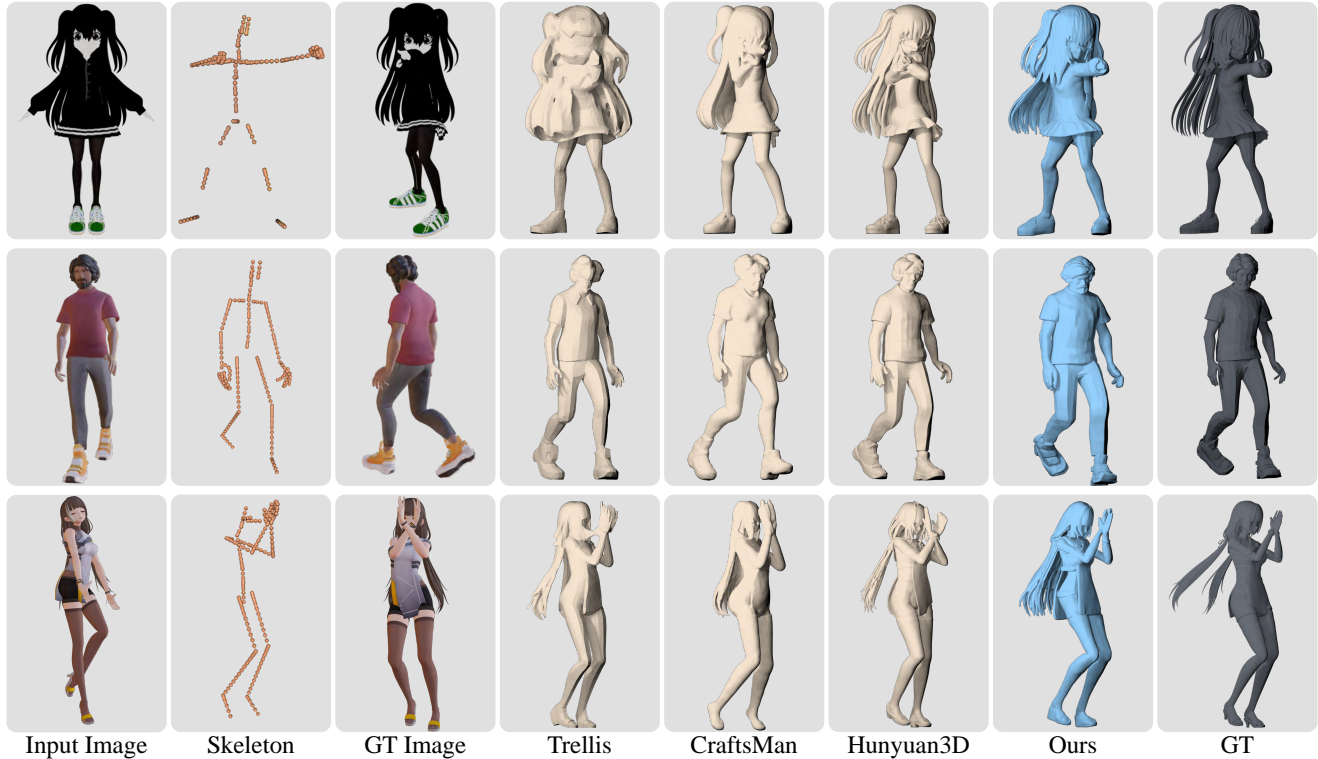


Figure 6. Qualitative comparison of arbitrary-pose stylization. For baselines, we utilize the target-pose images (GT image) as the input.

Table 2. Quantitative comparison for arbitrary-pose stylization from an arbitrary-pose image input. For the compared methods, we directly input the single-view target-pose image while inputting an arbitrary-pose image for our method.

Method	MAE ↓	SIM ↑	Uni3D-I ↑	ULIP-I ↑
Trellis [58]	7.20	0.904	0.306	0.164
CraftsMan [32]	7.66	0.895	0.291	0.146
Hunyuan3D 2.1 [22]	6.75	0.911	0.285	0.159
PoseMaster (Ours)	5.28	0.935	0.313	0.172

To conduct a rigorous comparison, we establish a highly competitive setting for the 3D native generation methods, including Trellis [58], CraftsMan [32], and Hunyuan3D 2.1 [22]. Specifically, we provide these baselines with the target-pose image in our testing dataset, completely eliminating any confounding factors or artifacts arising from 2D pose transfer steps. Meanwhile, our PoseMaster takes the source-pose image and the target-pose 3D skeleton as inputs. Despite the baselines having access to the target-pose image, PoseMaster still demonstrates superior performance in both quantitative and qualitative comparisons, as shown in Table 2 and Figure 6. This outcome underscores the fundamental limitation of purely image-conditioned baselines in resolving topological ambiguities caused by self-occlusion. By explicitly anchoring the generation process

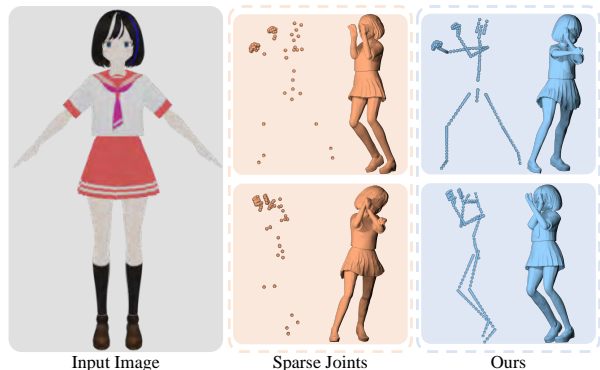


Figure 7. The qualitative comparison between different pose representations in terms of joints and bones of the skeleton.

to a 3D skeletal prior, PoseMaster reliably deduces coherent global geometry, facilitating topologically robust and complex pose stylizations.

5.3. Ablation Study

5.3.1. Effect of Pose Representation

We further investigate the impact of pose representation by comparing conventional sparse joint representations against our proposed dense point clouds. As illustrated in Fig. 7, sparse joints often fail to adequately convey complex artic-

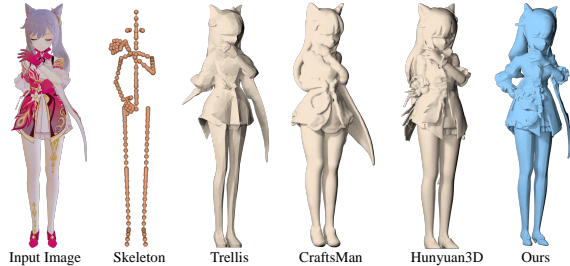


Figure 8. The ablation study for the importance of skeleton guidance in 3D generation.

Table 3. Quantitative comparison for skeleton guidance. With the skeleton guidance, our method achieves better performance in the task of image-to-3D generation.

Method	MAE ↓	SIM ↑	Uni3D-I ↑	ULIP-I ↑
Trellis [58]	7.53	0.898	0.303	0.153
CraftsMan [32]	8.01	0.893	0.304	0.152
Hunyuan3D 2.1 [22]	6.56	0.916	0.301	0.154
PoseMaster (Ours)	4.82	0.946	0.315	0.158

ulations, resulting in severe geometric and topological ambiguities. By interpolating the skeletal graph into a dense point cloud augmented with explicit directional vectors, our representation effectively injects robust structural and topological priors into the generation process. This explicitly alleviates the representational burden, enabling the highly accurate reconstruction of complex poses.

5.3.2. Impact of Explicit Skeleton Guidance

In this ablation study, we isolate and validate the fundamental benefits of explicit 3D skeleton guidance within native 3D generation frameworks. To this end, we provide state-of-the-art native 3D baselines (CraftsMan [32], Trellis [58], and Hunyuan3D 2.1 [22]) with only the input image, whereas our PoseMaster is conditioned on the aligned image and 3D skeleton. As reported in Table 3, our method yields consistently superior geometric accuracy. Furthermore, the qualitative comparisons in Figure 8 confirm that the integrated skeleton acts as a robust geometric anchor in 3D space. This explicit structural prior effectively resolves the depth ambiguity and spatial uncertainty inherent to monocular 3D reconstruction, significantly mitigating geometric collapse, particularly in self-occluded regions.

6. Application

One compelling application of our method lies in generating rigged meshes to facilitate the creation of animatable 3D assets. Prior rigging approaches, such as UniRig [69] and Puppeteer [52], typically employ auto-regressive (AR) models to predict an underlying skeleton from an input mesh. While these methods successfully generate skele-

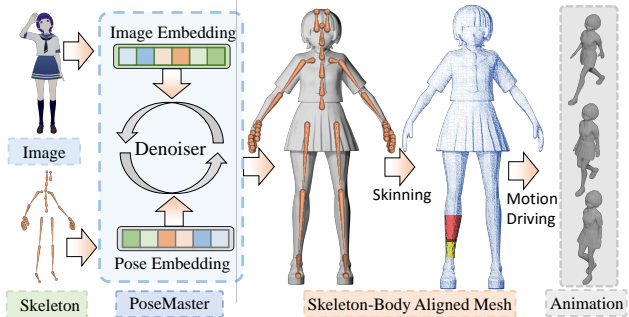


Figure 9. The application of our PoseMaster for animation. Our method can generate the skeleton-body alignment mesh, which can be easily used to animate by introducing a skinning model.

tons that are spatially aligned with the input geometry, they inherently suffer from limited controllability, often struggling to produce the specific skeletal hierarchies desired by users. In contrast, PoseMaster takes a user-specified skeleton as direct input and synthesizes a mesh that strictly conforms to its spatial layout. Consequently, it naturally functions as a highly controllable rigging model, fundamentally circumventing the uncontrollability bottlenecks of the AR paradigm. Furthermore, as illustrated in Figure 9, conditioning the generation on a user-provided skeleton enables seamless integration with standard skinning models, allowing the generated assets to be directly driven by existing motion sequences. This elegantly eliminates the tedious motion retargeting procedures typically required for animating newly generated 3D assets, thereby demonstrating significant practical advantages over prior AR-based methods.

7. Conclusion

In this paper, we introduce PoseMaster, a unified native 3D generation framework tailored for arbitrary pose stylization. Unlike conventional cascaded pipelines that rely on 2D foundation models for intermediate pose transfer prior to 3D generation, our approach seamlessly integrates pose stylization and 3D synthesis into a cohesive, end-to-end architecture. This paradigm shift circumvents the limitations of 2D skeleton conditions by directly leveraging explicit 3D skeletons, thereby providing the network with unambiguous spatial constraints and rigorous topological relationships. Consequently, the model’s capacity to faithfully synthesize complex target poses is significantly enhanced. Furthermore, we develop a scalable data engine to curate a large-scale, highly diverse dataset composed of pose-decoupled “Image-Skeleton-Mesh” triplets. Empowered by these innovations, PoseMaster not only establishes a new state-of-the-art in pose canonicalization but also demonstrates unprecedented robustness and versatility in synthesizing high-fidelity 3D assets across arbitrary, in-the-wild poses.

8. Acknowledgments

We gratefully acknowledge Xin Huang, Xin Yang, and Bowen Zhang for their assistance with texture generation, and the Tencent IEG VisVise Team for data rendering. We also thank the Tencent Hunyuan 3D Team for their generous support and collaboration throughout this project.

References

- [1] Gpt4-o, 2025. <https://openai.com/index/hello-gpt-4o/>. 2
- [2] Nanobanana, 2025. <https://aistudio.google.com/models/gemini-2-5-flash-image/>. 2
- [3] Readyplayerme, 2025. <https://readyplayer.me/>. 2, 4, 12
- [4] Blender, 2025. <https://www.blender.org/>. 15
- [5] Playbox, 2025. <https://www.aplaybox.com/>. 4, 12
- [6] Seed, 2025. <https://www.doubao.com/>. 2
- [7] Vroid-hub, 2025. <https://hub.vroid.com/>. 2, 4, 6, 12
- [8] Anonymous. Voxset: Sparse voxel set tokenizer for 3d shape generation. In *Submitted to The Fourteenth International Conference on Learning Representations*, 2025. under review. 3
- [9] Yukang Cao, Yan-Pei Cao, Kai Han, Ying Shan, and Kwan-Yee K Wong. Dreamavatar: Text-and-shape guided 3d human avatar generation via diffusion models. *arXiv preprint arXiv:2304.00916*, 2023. 2
- [10] Zhe Cao, Gines Hidalgo, Tomas Simon, Shih-En Wei, and Yaser Sheikh. Openpose: Realtime multi-person 2d pose estimation using part affinity fields. *IEEE transactions on pattern analysis and machine intelligence*, 43(1):172–186, 2019. 2, 4, 12
- [11] Chia-Hao Chen, Zi-Xin Zou, Yan-Pei Cao, Ze Yuan, Guan Luo, Xiaojuan Qi, Ding Liang, Song-Hai Zhang, and Yuan-Chen Guo. Lafite: A generative latent field for 3d native texturing. *arXiv preprint arXiv:2512.04786*, 2025. 14
- [12] Yiwen Chen, Zhihao Li, Yikai Wang, Hu Zhang, Qin Li, Chi Zhang, and Guosheng Lin. Ultra3d: Efficient and high-fidelity 3d generation with part attention. *arXiv preprint arXiv:2507.17745*, 2025. 3
- [13] Zhiqin Chen and Hao Zhang. Learning implicit fields for generative shape modeling. In *CVPR*, pages 5939–5948, 2019. 3
- [14] Zhaoxi Chen, Jiaxiang Tang, Yuhao Dong, Ziang Cao, Fangzhou Hong, Yushi Lan, Tengfei Wang, Haozhe Xie, Tong Wu, Shunsuke Saito, Liang Pan, Dahua Lin, and Ziwei Liu. 3dtopia-xl: High-quality 3d pbr asset generation via primitive diffusion. *arXiv preprint arXiv:2409.12957*, 2024. 3
- [15] Zedong Chu, Feng Xiong, Meiduo Liu, Jinzhi Zhang, Mingqi Shao, Zhaoxu Sun, Di Wang, and Mu Xu. Humanrig: Learning automatic rigging for humanoid character in a large scale dataset. In *Proceedings of the Computer Vision and Pattern Recognition Conference*, pages 304–313, 2025. 4
- [16] Matt Deitke, Ruoshi Liu, Matthew Wallingford, Huong Ngo, Oscar Michel, Aditya Kusupati, Alan Fan, Christian Laforte, Vikram Voleti, Samir Yitzhak Gadre, et al. Objaverse-xl: A universe of 10m+ 3d objects. *Advances in Neural Information Processing Systems*, 36:35799–35813, 2023. 4
- [17] Matt Deitke, Dustin Schwenk, Jordi Salvador, Luca Weihs, Oscar Michel, Eli VanderBilt, Ludwig Schmidt, Kiana Ehsani, Aniruddha Kembhavi, and Ali Farhadi. Objaverse: A universe of annotated 3d objects. In *Proceedings of the IEEE/CVF conference on computer vision and pattern recognition*, pages 13142–13153, 2023. 4
- [18] Xiao Fu, Wei Yin, Mu Hu, Kaixuan Wang, Yuexin Ma, Ping Tan, Shaojie Shen, Dahua Lin, and Xiaoxiao Long. Geowizard: Unleashing the diffusion priors for 3d geometry estimation from a single image. In *European Conference on Computer Vision*, pages 241–258. Springer, 2024. 5
- [19] Yuze He, Yanning Zhou, Wang Zhao, Zhongkai Wu, Kaiwen Xiao, Wei Yang, Yong-Jin Liu, and Xiao Han. Stdgen: Semantic-decomposed 3d character generation from single images. *arXiv preprint arXiv:2411.05738*, 2024. 2, 3, 4, 6, 13, 15
- [20] Yicong Hong, Kai Zhang, Jiuxiang Gu, Sai Bi, Yang Zhou, Difan Liu, Feng Liu, Kalyan Sunkavalli, Trung Bui, and Hao Tan. Lrm: Large reconstruction model for single image to 3d. *arXiv preprint arXiv:2311.04400*, 2023. 3
- [21] Li Hu. Animate anyone: Consistent and controllable image-to-video synthesis for character animation. In *Proceedings of the IEEE/CVF Conference on Computer Vision and Pattern Recognition*, pages 8153–8163, 2024. 2, 6
- [22] Team Hunyuan3D, Shuhui Yang, Mingxin Yang, Yifei Feng, Xin Huang, Sheng Zhang, Zebin He, Di Luo, Haolin Liu, Yunfei Zhao, et al. Hunyuan3d 2.1: From images to high-fidelity 3d assets with production-ready pbr material. *arXiv preprint arXiv:2506.15442*, 2025. 3, 4, 5, 6, 7, 8, 12, 15
- [23] Ruixiang Jiang, Can Wang, Jingbo Zhang, Menglei Chai, Mingming He, Dongdong Chen, and Jing Liao. Avatarcraft: Transforming text into neural human avatars with parameterized shape and pose control. In *Proceedings of the IEEE/CVF International Conference on Computer Vision*, pages 14371–14382, 2023. 2
- [24] Bingxin Ke, Kevin Qu, Tianfu Wang, Nando Metzger, Shengyu Huang, Bo Li, Anton Obukhov, and Konrad Schindler. Marigold: Affordable adaptation of diffusion-based image generators for image analysis. *arXiv preprint arXiv:2505.09358*, 2025. 5
- [25] Nikos Kolotouros, Thiemo Alldieck, Andrei Zanfir, Eduard Bazavan, Mihai Fieraru, and Cristian Sminchisescu. Dreamhuman: Animatable 3d avatars from text. *Advances in Neural Information Processing Systems*, 36:10516–10529, 2023. 2
- [26] Zeqiang Lai, Yunfei Zhao, Haolin Liu, Zibo Zhao, Qingxiang Lin, Huiwen Shi, Xianghui Yang, Mingxin Yang, Shuhui Yang, Yifei Feng, et al. Hunyuan3d 2.5: Towards high-fidelity 3d assets generation with ultimate details. *arXiv preprint arXiv:2506.16504*, 2025. 14, 15
- [27] Zeqiang Lai, Yunfei Zhao, Zibo Zhao, Xin Yang, Xin Huang, Jingwei Huang, Xiangyu Yue, and Chunchao Guo. Natex: Seamless texture generation as latent color diffusion. *arXiv preprint arXiv:2511.16317*, 2025. 14
- [28] Yushi Lan, Fangzhou Hong, Shuai Yang, Shangchen Zhou, Xuyi Meng, Bo Dai, Xingang Pan, and Chen Change Loy.

- Ln3diff: Scalable latent neural fields diffusion for speedy 3d generation. In *ECCV*, 2024. 3
- [29] Yushi Lan, Shangchen Zhou, Zhaoyang Lyu, Fangzhou Hong, Shuai Yang, Bo Dai, Xingang Pan, and Chen Change Loy. Gaussiananything: Interactive point cloud latent diffusion for 3d generation. In *ICLR*, 2025. 3
- [30] Chun-Liang Li, Manzil Zaheer, Yang Zhang, Barnabas Poczos, and Ruslan Salakhutdinov. Point cloud gan. *arXiv preprint arXiv:1810.05795*, 2018. 3
- [31] Peng Li, Yuan Liu, Xiaoxiao Long, Feihu Zhang, Cheng Lin, Mengfei Li, Xingqun Qi, Shanghang Zhang, Wenhan Luo, Ping Tan, et al. Era3d: High-resolution multiview diffusion using efficient row-wise attention. *arXiv preprint arXiv:2405.11616*, 2024. 3
- [32] Weiyu Li, Jiarui Liu, Rui Chen, Yixun Liang, Xuelin Chen, Ping Tan, and Xiaoxiao Long. Craftsman: High-fidelity mesh generation with 3d native generation and interactive geometry refiner. *arXiv preprint arXiv:2405.14979*, 2024. 3, 4, 6, 7, 8, 12
- [33] Weiyu Li, Xuanyang Zhang, Zheng Sun, Di Qi, Hao Li, Wei Cheng, Weiwei Cai, Shihao Wu, Jiarui Liu, Zihao Wang, et al. Step1x-3d: Towards high-fidelity and controllable generation of textured 3d assets. *arXiv preprint arXiv:2505.07747*, 2025. 3
- [34] Yangguang Li, Zi-Xin Zou, Zexiang Liu, Dehu Wang, Yuan Liang, Zhipeng Yu, Xingchao Liu, Yuan-Chen Guo, Ding Liang, Wanli Ouyang, and Yan-Pei Cao. Triposg: High-fidelity 3d shape synthesis using large-scale rectified flow models. *CoRR*, abs/2502.06608, 2025. 3
- [35] Zhihao Li, Yufei Wang, Heliang Zheng, Yihao Luo, and Bihan Wen. Sparc3d: Sparse representation and construction for high-resolution 3d shapes modeling. *arXiv preprint arXiv:2505.14521*, 2025. 15
- [36] Yixun Liang, Kunming Luo, Xiao Chen, Rui Chen, Hongyu Yan, Weiyu Li, Jiarui Liu, and Ping Tan. Unitex: Universal high fidelity generative texturing for 3d shapes. *arXiv preprint arXiv:2505.23253*, 2025. 14
- [37] Tingting Liao, Hongwei Yi, Yuliang Xiu, Jiayang Tang, Yangyi Huang, Justus Thies, and Michael J Black. Tada! text to animatable digital avatars. In *2024 International Conference on 3D Vision (3DV)*, pages 1508–1519. IEEE, 2024. 2
- [38] Xingchao Liu, Chengyue Gong, and Qiang Liu. Flow straight and fast: Learning to generate and transfer data with rectified flow. *arXiv preprint arXiv:2209.03003*, 2022. 3
- [39] Ziwei Liu, Ping Luo, Shi Qiu, Xiaogang Wang, and Xiaoou Tang. Deepfashion: Powering robust clothes recognition and retrieval with rich annotations. In *Proceedings of IEEE Conference on Computer Vision and Pattern Recognition (CVPR)*, 2016. 15, 16
- [40] Zhen Liu, Yao Feng, Michael J. Black, Derek Nowrouzezahrai, Liam Paull, and Weiyang Liu. Meshdiffusion: Score-based generative 3d mesh modeling. In *International Conference on Learning Representations*, 2023. 3
- [41] Xiaoxiao Long, Yuan-Chen Guo, Cheng Lin, Yuan Liu, Zhiyang Dou, Lingjie Liu, Yuexin Ma, Song-Hai Zhang, Marc Habermann, Christian Theobalt, et al. Wonder3d: Single image to 3d using cross-domain diffusion. *arXiv preprint arXiv:2310.15008*, 2023. 3
- [42] Kunming Luo, Hongyu Yan, Yuan Liu, Zihao Zhang, Manyuan Zhang, Wenping Wang, and Ping Tan. Ctr3d: Cross-view token reduction for dense multi-view generation. In *Thirteenth International Conference on 3D Vision*. 3
- [43] Charlie Nash, Yaroslav Ganin, SM Ali Eslami, and Peter Battaglia. Polygen: An autoregressive generative model of 3d meshes. In *International conference on machine learning*, pages 7220–7229. PMLR, 2020. 3
- [44] Maxime Oquab, Timothée Darcet, Theo Moutakanni, Huy V. Vo, Marc Szafraniec, Vasil Khalidov, Pierre Fernandez, Daniel Haziza, Francisco Massa, Alaaeldin El-Nouby, Russell Howes, Po-Yao Huang, Hu Xu, Vasu Sharma, Shangwen Li, Wojciech Galuba, Mike Rabbat, Mido Assran, Nicolas Ballas, Gabriel Synnaeve, Ishan Misra, Herve Jegou, Julien Mairal, Patrick Labatut, Armand Joulin, and Piotr Bojanowski. Dinov2: Learning robust visual features without supervision, 2023. 5
- [45] Jeong Joon Park, Peter Florence, Julian Straub, Richard Newcombe, and Steven Lovegrove. DeepSDF: Learning continuous signed distance functions for shape representation. In *CVPR*, pages 165–174, 2019. 3
- [46] Bohao Peng, Jian Wang, Yuechen Zhang, Wenbo Li, Ming-Chang Yang, and Jiaya Jia. Controlnext: Powerful and efficient control for image and video generation. *arXiv preprint arXiv:2408.06070*, 2024. 2
- [47] Hao-Yang Peng, Jia-Peng Zhang, Meng-Hao Guo, Yan-Pei Cao, and Shi-Min Hu. Charactergen: Efficient 3d character generation from single images with multi-view pose canonicalization. *ACM Transactions on Graphics (TOG)*, 43(4): 1–13, 2024. 2, 3, 4, 6, 12, 13, 15, 18
- [48] Charles Ruizhongtai Qi, Li Yi, Hao Su, and Leonidas J Guibas. Pointnet++: Deep hierarchical feature learning on point sets in a metric space. *Advances in neural information processing systems*, 30, 2017. 5
- [49] Xuanchi Ren, Jiahui Huang, Xiaohui Zeng, Ken Museth, Sanja Fidler, and Francis Williams. Xcube: Large-scale 3d generative modeling using sparse voxel hierarchies. In *Proceedings of the IEEE/CVF Conference on Computer Vision and Pattern Recognition*, 2024. 3
- [50] Robin Rombach, Andreas Blattmann, Dominik Lorenz, Patrick Esser, and Björn Ommer. High-resolution image synthesis with latent diffusion models. In *CVPR*, 2022. 2
- [51] Yawar Siddiqui, Antonio Alliegro, Alexey Artemov, Tatiana Tommasi, Daniele Sirigatti, Vladislav Rosov, Angela Dai, and Matthias Nießner. Meshgpt: Generating triangle meshes with decoder-only transformers. In *Proceedings of the IEEE/CVF conference on computer vision and pattern recognition*, pages 19615–19625, 2024. 3
- [52] Chaoyue Song, Xiu Li, Fan Yang, Zhongcong Xu, Jiacheng Wei, Fayao Liu, Jiashi Feng, Guosheng Lin, and Jianfeng Zhang. Puppeteer: Rig and animate your 3d models. *Advances in Neural Information Processing Systems*, 2025. 8
- [53] Shuai Tan, Biao Gong, Xiang Wang, Shiwei Zhang, Dandan Zheng, Ruobing Zheng, Kecheng Zheng, Jingdong Chen,

- and Ming Yang. Animate-x: Universal character image animation with enhanced motion representation. *arXiv preprint arXiv:2410.10306*, 2024. 2, 12
- [54] Xiang Wang, Shiwei Zhang, Changxin Gao, Jiayu Wang, Xiaoqiang Zhou, Yingya Zhang, Luxin Yan, and Nong Sang. Unianimate: Taming unified video diffusion models for consistent human image animation. *arXiv preprint arXiv:2406.01188*, 2024. 2, 6
- [55] Chenfei Wu, Jiahao Li, Jingren Zhou, Junyang Lin, Kaiyuan Gao, Kun Yan, Sheng-ming Yin, Shuai Bai, Xiao Xu, Yilei Chen, et al. Qwen-image technical report. *arXiv preprint arXiv:2508.02324*, 2025. 2, 12, 13, 14, 15
- [56] Shuang Wu, Youtian Lin, Feihu Zhang, Yifei Zeng, Jingxi Xu, Philip Torr, Xun Cao, and Yao Yao. Direct3d: Scalable image-to-3d generation via 3d latent diffusion transformer. *arXiv preprint arXiv:2405.14832*, 2024. 3
- [57] Shuang Wu, Youtian Lin, Feihu Zhang, Yifei Zeng, Yikang Yang, Yajie Bao, Jiachen Qian, Siyu Zhu, Xun Cao, Philip Torr, and Yao Yao. Direct3d-s2: Gigascale 3d generation made easy with spatial sparse attention. *CoRR*, abs/2505.17412, 2025. 3, 15
- [58] Jianfeng Xiang, Zelong Lv, Sicheng Xu, Yu Deng, Ruicheng Wang, Bowen Zhang, Dong Chen, Xin Tong, and Jialong Yang. Structured 3d latents for scalable and versatile 3d generation. In *Proceedings of the Computer Vision and Pattern Recognition Conference*, pages 21469–21480, 2025. 3, 6, 7, 8, 12
- [59] Yiming Xie, Varun Jampani, Lei Zhong, Deqing Sun, and Huaizu Jiang. Omnicontrol: Control any joint at any time for human motion generation. *arXiv preprint arXiv:2310.08580*, 2023. 2
- [60] Shuolin Xu, Siming Zheng, Ziyi Wang, HC Yu, Jinwei Chen, Huaqi Zhang, Bo Li, and Peng-Tao Jiang. Hypermotion: Dit-based pose-guided human image animation of complex motions, 2025. 2
- [61] Yuanyou Xu, Zongxin Yang, and Yi Yang. Skdream: Controllable multi-view and 3d generation with arbitrary skeletons. In *Proceedings of the Computer Vision and Pattern Recognition Conference*, pages 314–325, 2025. 2, 3, 6
- [62] Le Xue, Mingfei Gao, Chen Xing, Roberto Martín-Martín, Jiajun Wu, Caiming Xiong, Ran Xu, Juan Carlos Niebles, and Silvio Savarese. Ulip: Learning a unified representation of language, images, and point clouds for 3d understanding. In *Proceedings of the IEEE/CVF conference on computer vision and pattern recognition*, pages 1179–1189, 2023. 5
- [63] Hongyu Yan, Zijun Li, Kunming Luo, Li Lu, and Ping Tan. Symmcompletion: High-fidelity and high-consistency point cloud completion with symmetry guidance. In *Proceedings of the AAAI Conference on Artificial Intelligence*, pages 9094–9102, 2025. 5
- [64] Xuejun Yan, Hongyu Yan, Jingjing Wang, Hang Du, Zhihong Wu, Di Xie, Shiliang Pu, and Li Lu. Fbnet: Feedback network for point cloud completion. In *European conference on computer vision*, pages 676–693. Springer, 2022. 5
- [65] Guandao Yang, Xun Huang, Zekun Hao, Ming-Yu Liu, Serge Belongie, and Bharath Hariharan. Pointflow: 3d point cloud generation with continuous normalizing flows. *arXiv*, 2019. 3
- [66] Chongjie Ye, Yushuang Wu, Ziteng Lu, Jiahao Chang, Xiaoyang Guo, Jiaqing Zhou, Hao Zhao, and Xiaoguang Han. Hi3dgen: High-fidelity 3d geometry generation from images via normal bridging. *arXiv preprint arXiv:2503.22236*, 2025. 3
- [67] Biao Zhang, Jiapeng Tang, Matthias Niessner, and Peter Wonka. 3dshape2vecset: A 3d shape representation for neural fields and generative diffusion models. *ACM Transactions on Graphics (TOG)*, 42(4):1–16, 2023. 3
- [68] Huichao Zhang, Bowen Chen, Hao Yang, Liao Qu, Xu Wang, Li Chen, Chao Long, Feida Zhu, Kang Du, and Min Zheng. Avatarverse: High-quality & stable 3d avatar creation from text and pose. 2023. 2
- [69] Jia-Peng Zhang, Cheng-Feng Pu, Meng-Hao Guo, Yan-Pei Cao, and Shi-Min Hu. One model to rig them all: Diverse skeleton rigging with unirig. *ACM Trans. Graph.*, 44(4), 2025. 8, 12
- [70] Lvmin Zhang, Anyi Rao, and Maneesh Agrawala. Adding conditional control to text-to-image diffusion models. In *Proceedings of the IEEE/CVF international conference on computer vision*, pages 3836–3847, 2023. 2, 6
- [71] Longwen Zhang, Ziyu Wang, Qixuan Zhang, Qiwei Qiu, Anqi Pang, Haoran Jiang, Wei Yang, Lan Xu, and Jingyi Yu. Clay: A controllable large-scale generative model for creating high-quality 3d assets. *ACM Transactions on Graphics (TOG)*, 43(4):1–20, 2024. 3, 4
- [72] Muxin Zhang, Qiao Feng, Zhuo Su, Chao Wen, Zhou Xue, and Kun Li. Joint2human: High-quality 3d human generation via compact spherical embedding of 3d joints. In *Proceedings of the IEEE/CVF Conference on Computer Vision and Pattern Recognition*, pages 1429–1438, 2024. 5
- [73] Xuanmeng Zhang, Jianfeng Zhang, Chenxu Zhang, Jun Hao Liew, Huichao Zhang, Yi Yang, and Jiashi Feng. Avatarstudio: High-fidelity and animatable 3d avatar creation from text. *International Journal of Computer Vision*, pages 1–19, 2025. 2
- [74] Yuxuan Zhang, Yirui Yuan, Yiren Song, Haofan Wang, and Jiaming Liu. Easycontrol: Adding efficient and flexible control for diffusion transformer. *arXiv preprint arXiv:2503.07027*, 2025. 2
- [75] Shihao Zhao, Dongdong Chen, Yen-Chun Chen, Jianmin Bao, Shaozhe Hao, Lu Yuan, and Kwan-Yee K Wong. Uni-controlnet: All-in-one control to text-to-image diffusion models. *Advances in Neural Information Processing Systems*, 36:11127–11150, 2023. 2
- [76] Zibo Zhao, Wen Liu, Xin Chen, Xianfang Zeng, Rui Wang, Pei Cheng, BIN FU, Tao Chen, Gang YU, and Shenghua Gao. Michelangelo: Conditional 3d shape generation based on shape-image-text aligned latent representation. In *NeurIPS*, 2023. 3
- [77] Junsheng Zhou, Jinsheng Wang, Baorui Ma, Yu-Shen Liu, Tiejun Huang, and Xinlong Wang. Uni3d: Exploring unified 3d representation at scale. *arXiv preprint arXiv:2310.06773*, 2023. 5
- [78] Linqi Zhou, Yilun Du, and Jiajun Wu. 3d shape generation and completion through point-voxel diffusion. In *Proceedings of the IEEE/CVF international conference on computer vision*, pages 5826–5835, 2021. 3

9. Additional Details

In this section, we provide additional details to clarify our method, including metric computation, data details, and skeleton definition.

9.1. Metric Computation

Given the sensitivity of Chamfer Distance (CD) to shape alignment and point distribution—particularly the topological discrepancies between watertight and non-watertight meshes—we adopt Mean Angular Error (MAE) and Cosine Similarity (SIM) of rendered normal maps to assess geometric accuracy. Specifically, our evaluation begins by rendering the front-view normal map of the predicted mesh. To account for potential azimuthal misalignments between the predicted meshes (including those generated by baseline methods such as Hunyuan3D 2.1 [22] and CraftsMan [32]) and the ground truth (GT) models, we render the GT normals across 36 azimuths uniformly sampled at 10° intervals (from 0° to 350°). We then compute the MAE and SIM between the predicted front-view normals and the GT normals under each viewpoint. The best-matching score among all views is reported as the final metric, ensuring a robust evaluation of geometric fidelity.

9.2. Data details.

Our constructed dataset comprises animatable dynamic assets and static assets in an approximate 3:2 ratio. For static meshes lacking skeletal structures, we employ an auto-regressive model fine-tuned from UniRig [69] for automatic rig generation. For the dynamic assets, the characters from ReadyPlayerMe [3] and VRoid [7] are driven by Mixamo motion sequences, whereas the assets from Playbox [5] are animated by VMD motion sequences compatible with the MMD data format.

Image rendering. For dynamic characters, we fix the camera azimuth, allowing the character’s articulated motions to naturally induce viewpoint variations. Furthermore, we randomize the camera elevation between 0° and 10° and dynamically adjust the camera distance to ensure the animated character remains centered in the viewpoint. For static meshes, we render four canonical views (front, back, left, and right) alongside 32 uniformly sampled random views. All renderings are generated using perspective projection.

9.3. Skeleton Definition

Following previous methods [47, 53] that utilize Openpose [10] for pose conditioning, we select the body’s bones and hand’s bones in the 3D skeleton as our skeleton system. This selection excludes hair and skirt bones, yet remains sufficient to define a humanoid pose effectively.

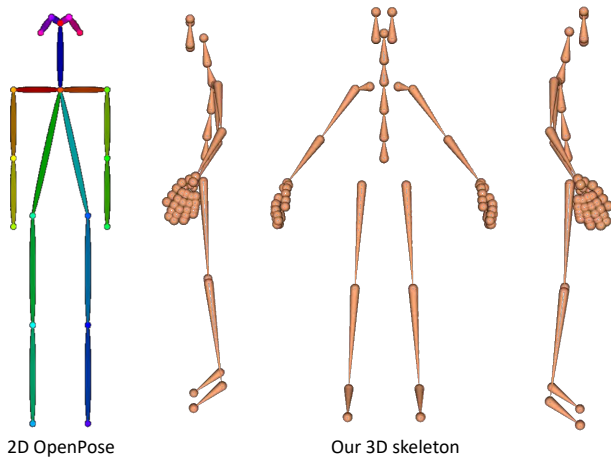


Figure 10. The visualization of the standard skeletons of Openpose [10] and ours (here, we take the skeleton from ReadyPlayerMe’s [3] data as the example).

Table 4. The quantitative comparison for arbitrary pose stylization by using the target-pose images edited from Qwen-Image [55] as the baselines’ input.

Method	MAE ↓	SIM ↑	Uni3D-I ↑	ULIP-I ↑
Trellis [58]	8.50	0.874	0.293	0.160
CraftsMan [32]	8.55	0.876	0.302	0.148
Hunyuan3D 2.1 [22]	8.15	0.874	0.293	0.160
PoseMaster (Ours)	5.28	0.935	0.313	0.172

10. Additional Experimental Results

In this section, we present extended comparative evaluations, featuring additional qualitative visualizations for both arbitrary-pose stylization and pose canonicalization. Following these comparisons, we provide a comprehensive analysis of the computational efficiency and structural robustness of our proposed framework. Finally, we report supplementary texture synthesis results and demonstrate a practical downstream application.

10.1. More results on Arbitrary-pose Stylization

To isolate the effects of 2D image distortion inherent in decoupled pose stylization pipelines, we utilized ground-truth target-pose images as inputs for existing 3D native methods (i.e., Trellis [58], CraftsMan [32], and Hunyuan3D 2.1 [22]) in the arbitrary-pose stylization comparisons presented in Sec. 5.2.2. Therefore, to explicitly expose the limitations of the decoupled paradigm—where 2D pose transformation and 3D generation are treated as independent stages—we construct a comprehensive baseline pipeline utilizing Qwen-Image [55] to synthesize target-pose inputs. Specifically, we project 3D skeletons into Openpose-style

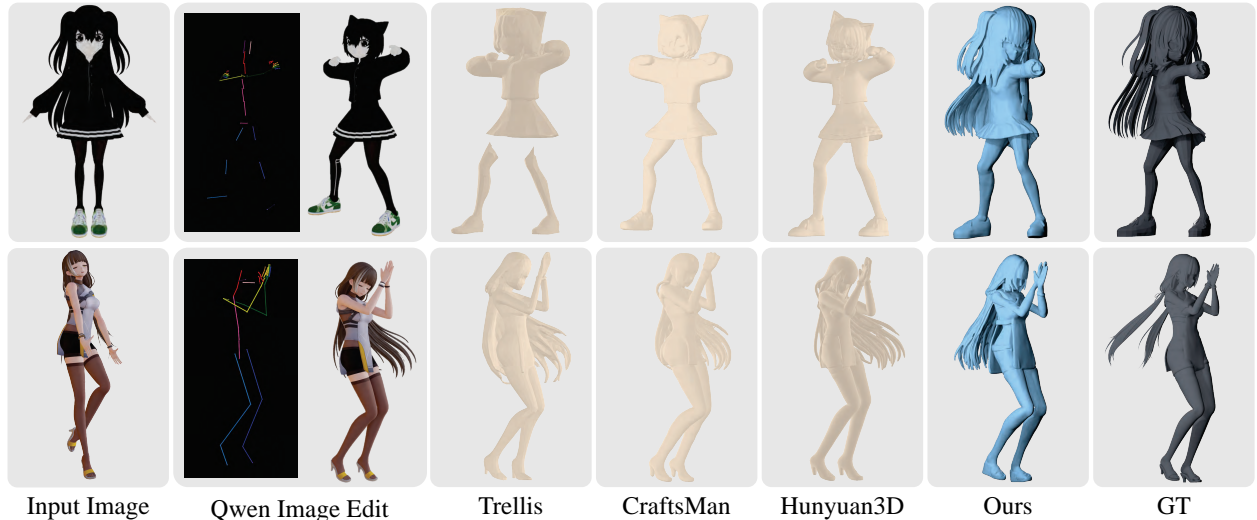


Figure 11. The qualitative comparison for arbitrary-pose stylization by using the target-pose images edited from Qwen-Image [55] as the baselines’ input.

Table 5. Time comparison of generation speed.

Method	CharacterGen [47]	StdGen [19]	Ours
Inference time	~ 32.98 (s)	~ 61.54 (s)	~ 23.48 (s)

2D skeleton maps to guide Qwen-Image in generating pose-edited images, which are subsequently fed into 3D generation models to produce meshes.

As shown in Table 4 and Figure 11, our method presents significant quantitative and qualitative superiority over both baseline methods. Visual inspection reveals that Qwen-Image-based editing frequently compromises the preservation of original identity features. Moreover, the 2D interpretation of skeletons suffers from viewpoint-dependent ambiguity, leading to geometric inaccuracies in the generated poses. Consequently, the performance of the Qwen-Image-based pipeline falls short of the setting that uses ground-truth inputs. This performance gap strongly underscores the critical necessity of a unified framework and explicit 3D skeleton guidance for robust 3D pose stylization.

Additional qualitative results for arbitrary-pose stylization are presented in Figure 18 and Figure 19. These visualizations further demonstrate the robustness of PoseMaster. By seamlessly integrating pose stylization and 3D generation into a unified generative framework, we achieve precise pose control directly in the 3D domain. Moreover, the incorporation of 3D skeletons facilitates accurate pose recovery and manipulation, substantially enhancing the model’s practical usability.

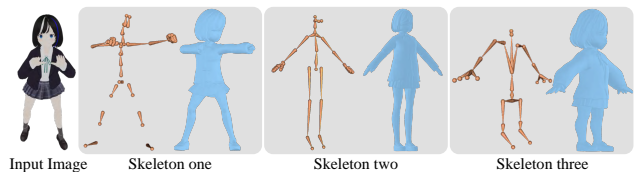


Figure 12. The visualization for robustness analysis.

10.2. Efficiency Analysis

We evaluate the computational efficiency of our method against previous multi-stage pose stylization approaches, including CharacterGen [47] and StdGen [19]. All inference timings are measured on a single NVIDIA H20 GPU. As detailed in Table 5, PoseMaster achieves faster generation speeds. This acceleration is primarily attributed to our integrated, single-stage generative framework, which streamlines the conventional multi-stage workflow and eliminates intermediate computational bottlenecks.

10.3. Robustness Analysis

In this section, we introduce various skeleton conditions to validate the robustness of our model. As illustrated in Figure 12, we design test cases featuring misaligned image-skeleton pairs with significant discrepancies in body proportions and topology. Remarkably, PoseMaster exhibits exceptional structural adherence. Even when conditioned on heavily mismatched skeletons, the model consistently synthesizes meshes that strictly conform to the target skeletal topology while faithfully preserving the appearance of the source image. This flexibility is particularly valuable for downstream game asset creation, such as character retarget-

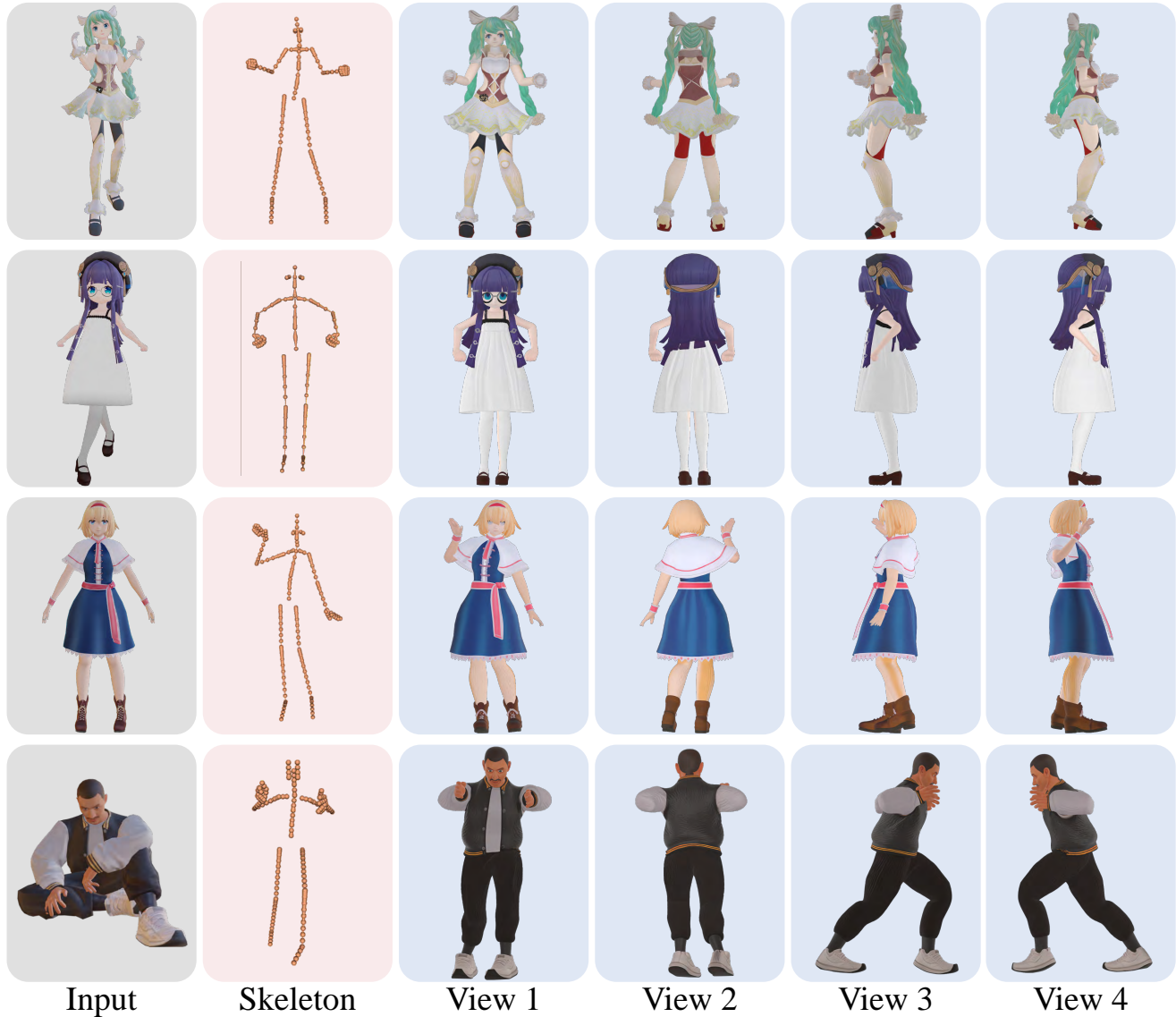


Figure 13. The visualized results for textured mesh. We employ 3D native texturing approaches to synthesize textures for the meshes generated by PoseMaster. The final textured assets are rendered from four canonical viewpoints.

ing and body proportion customization

10.4. Texture Generation

In this work, geometry and texture synthesis are formulated as decoupled tasks; hence, explicit texture generation remains orthogonal to our main contributions. To demonstrate the practical utility of our approach, we provide texturing results leveraging state-of-the-art models. While the inherent pose inconsistency between the input image and the generated geometry poses a substantial challenge for texture mapping, we mitigate this by integrating advanced image-editing models (e.g., Qwen-Image [55]) and 3D native texturing approaches (e.g., UniTEX [36], NaTex [27],

LaFiTe [11]). As depicted in Figure. 13, these frameworks demonstrate strong robustness against pose misalignment. For minor persistent artifacts, a promising future direction is to fine-tune these models specifically on misaligned image-geometry datasets. Note that we employ Hunyuan3D 2.5 [26] as an intermediate geometric refinement step prior to the texturing phase.

10.5. More Results on Pose Canonicalization

Results on in-the-wild images. To assess the zero-shot generalization capability of our model, we compile a diverse in-the-wild test set comprising both virtual avatars and real-world photographs. We evaluate our method against

CharacterGen [47], StdGEN [19], and Hunyuan3D 2.1 [22]. For the Hunyuan3D 2.1, we utilized Qwen-Image [55] to transform the pose of the images to form its inputs. To circumvent the instability of Qwen-Image in generating A-pose outputs, we prompted the model to synthesize T-pose images instead. As shown in the qualitative comparisons, our method exhibits superior pose customization and geometric fidelity. CharacterGen and StdGEN, which are predominantly trained on single-style VRoid data, struggle to generalize to diverse artistic styles; their generated A-pose images often suffer from severe artifacts and distortions, fundamentally bottlenecking the subsequent 3D reconstruction. While Qwen-Image can alleviate some 2D distortion, controlling poses purely via text descriptions introduces significant randomness. For instance, in the inputs generated for Hunyuan3D, although the overall posture approaches a T-pose, critical details such as arm elevation, leg spacing, and perspective lack precise control. In contrast, our end-to-end framework bypasses the error-prone 2D editing stage. By employing explicit 3D skeletons as conditioning, we achieve strictly standardized pose canonicalization. Furthermore, inheriting the powerful priors of native 3D generation models ensures high-fidelity mesh topologies.

Additionally, as illustrated in Figure 15, our method robustly handles real-world human images from the DeepFashion dataset [39]. The incorporation of a large-scale, diverse training dataset empowers our model to bridge the domain gap, significantly broadening its real-world applicability.

Results on AI-synthesized images. We further evaluate generalization on synthetic images produced by text-to-image models. As illustrated in Figure 16, PoseMaster exhibits superior stability in pose canonicalization tasks compared to pipeline-dependent approaches. Notably, for the Hunyuan3D baseline, the required T-pose inputs were synthesized via text-prompted Qwen-Image, which often struggles with complex pose transformations.

Results on CharacterGen’s testing set. For a rigorous and fair comparison, we evaluate our method on the official test set provided by CharacterGen [47]. As shown in Figure 17, PoseMaster significantly outperforms both CharacterGen and StdGen [19] in terms of geometric quality and pose accuracy, further validating that native pose stylization yields optimal results for pose canonicalization.

10.6. Application in 3D Printing

Leveraging our arbitrary-pose stylization capabilities, we demonstrate a practical downstream application: a customized 3D printing pipeline for stylized anime characters. As depicted in Figure 14, the workflow begins with a 2D anime character generated via text-to-image models. Users can then author desired poses using standard tools like Blender [4] or Openpose Editor. By extracting the 3D

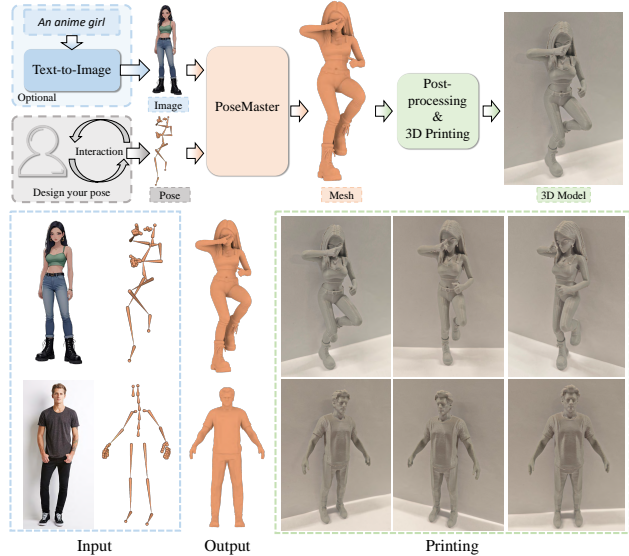


Figure 14. The system of 3D printing based on our PoseMaster. PoseMaster can customize the pose of a character from a single image for figure printing.

skeleton from the authored pose, PoseMaster directly reconstructs a 3D character mesh matching both the input identity and the target pose. Following standard post-processing, the stylized mesh is readily 3D-printed.

11. Limitation and Discussion

First, we acknowledge that native 3D pose stylization remains a highly challenging task. While our framework demonstrates strong overall pose controllability, synthesizing fine-grained geometric details—such as intricate hand gestures, flowing skirts, and complex hairstyles—requires further exploration. Furthermore, our current implementation utilizes a single-stage generation paradigm operating at a spatial resolution of 512. Consequently, the high-frequency geometric fidelity of our outputs may lag behind recent state-of-the-art multi-stage refinement methods (e.g., Direct3D-S2 [57], Hunyuan3D 2.5 [26], and Sparc3D [35]). A promising avenue for future work is to integrate a high-resolution geometric refinement module to upscale and enhance the coarse meshes generated in the first stage, thereby achieving photorealistic and highly detailed pose stylization.



Figure 15. The qualitative comparison for pose canonicalization on real-world images from the DeepFashion dataset [39].



Figure 16. The qualitative comparison for pose canonicalization on AI-synthesized images.



Figure 17. The qualitative comparison for pose canonicalization on CharacterGen’s [47] testing dataset.



Figure 18. The qualitative results for arbitrary-pose stylization.



Figure 19. The qualitative results for arbitrary-pose stylization.